Hazelnut quality detection based on deep learning and near-infrared spectroscopy

Dandan Li, Dongyan Zhang, Dapeng Jiang, Jun Cao and Jiuqing Liu

College of Mechanical and Electrical Engineering, Northeast Forestry University, Harbin 150040, Heilongjiang, China

Received: 03.09.2022

Abstract. Hazelnut kernels can often be incomplete or malformed and have some other defects. Manual methods for their classification and recognition or even old-fashioned machine-learning approaches are prone to the problems of low recognition efficiency and high misjudgement rates. In this study we apply deep learning to the problem of recognition of hazelnut-kernel defects. Two convolution neural-network systems, MobileNetV2 and Resnet-50, are used for training and recognition. It is found that the prediction accuracy of the ResNet-50 training set is improved by 10.3% and the training-loss rate reduced by 0.041, if compared with MobileNetV2. Moreover, the validation accuracy achieved with ResNet-50 is higher by 13.9% and the validation-loss rate lower by 0.151. This proves that the overall training effect of the Resnet-50 neural network is better than that of MobileNetV2. Basing on the near-infrared absorption spectroscopy, we also detect the protein content in hazelnuts, which represents an important parameter for evaluating their quality. A Kennard–Stone algorithm is used to classify a sample set. To elaborate a technique for the quantitative protein analysis of hazelnuts, we employ a partial least-squares method. The appropriate spectral data is preprocessed according to the methods of first derivative, second derivative and standard normal variate. The effect of these methods on the accuracy are compared. The results demonstrate that the model based on the first derivative is the best in case of the data referred to the overall spectral range. The correlation coefficients for the training and test sets are respectively equal to 0.938 and 0.965, whereas the root-mean-square errors for these sets amount respectively to 0.286 and 0.577. Our study testifies that the protein content in hazelnuts can be quickly and nondestructively detected using the near-infrared spectroscopy.

Keywords: neural networks, deep learning, partial least-squares method, near-infrared spectroscopy, nondestructive testing, protein content

UDC: 535-1+630*8+004.93

1. Introduction

Hazelnut is known to be rich in proteins, lipids, sugars, carotene, vitamins B_1, B_2 and E, as well as eight kinds of amino acids needed by a human body. The amounts of calcium, phosphorus, iron, and some other nutritional elements in hazelnuts is higher than that in the other nuts [1]. Hazelnut is not only a delicious snack loved by many people but can also be added to chocolate, candy and bread [2, 3]. Being a valuable source of proteins and lipids, it is often called a "king of nuts" [4, 5].

Hazelnuts are affected by climatic environment and storage factors and have often the problems of low yield, small size, deformity and high percentage of incomplete nuts. These problems deteriorate the quality of hazelnuts and affect seriously their subsequent processing and consumption [6].

Common techniques used for the classification of hazelnut kernels are based on manual selection, which is inefficient, while standard discrimination methods are difficult to unify and prone

to mistakes, such that a high-quality level of hazelnut kernels cannot be ensured. Many scholars have studied the problems of classification of kernels and recognition of crop defects for the nuts and seeds. As a result, great progress in the field has been achieved [2, 3]. The researchers have used computers to classify agricultural products, thus providing high speed of the recognition and classification. However, standard classification methods reveal evident shortcomings. For instance, the efficiency of manually selected image features is usually low, the characteristics of image extraction are not obvious, and the efficiency of image recognition and classification is low. A rapid development of deep learning and associated computer technologies in the recent years has provided significant success in image classification and object detection. The work concerned with deep learning and based upon convolutional neural networks is now in full swing. Deep-learning algorithms have natural advantages over many other methods in terms of automatic feature extraction and representation of raw data. Moreover, they manifest strong fitting and inclusion abilities. In the present study, we suggest the deep learning for detecting defects of hazelnut kernels.

He Yizhi et al. [7] have offered a method for recognition of lemon defects, which is based on the deep learning. A vgg16-based convolutional neural network has been constructed to train preprocessed data. The appropriate experiments have shown that the accuracy of the model in the verification set is 95.44%, which is much higher than that typical for the traditional k-nearest neighbour and support vector-machine methods. Basing on transfer learning, Li Cong et al. [8] have suggested an improved RESNET network TL-ROI-X-ResNext-50 classification model for recognizing defects of Hami jujube. Their experiments have demonstrated that the method can significantly reduce the amount of calculations, improve the recognition accuracy and meet better the main production requirements.

Protein accounts for more than 20% of hazelnut kernels [9]. It provides an important index to judge the quality of hazelnut kernels. To determine the protein content, a Kjeldahl nitrogen method is usually used, although it is destructive. This method employs time-consuming, laborious and cumbersome operations. Moreover, a toxic gas released during the process is harmful to laboratory personnel, while the corresponding environmental pollution is large enough [10, 11]. Therefore, it would be very important to develop a nondestructive, harmless, simple and rapid method for detecting the hazelnut-protein content.

A near-infrared spectroscopy (NIRS) is a well-known method of qualitative or quantitative analyses of organic chemicals, which uses the optical-response characteristics of these chemicals in the near-infrared spectral range and can be combined with stoichiometric methods. It is a nondestructive, low-cost and rapid method that causes no pollution. A spectral absorption band in the near-infrared range typically represents a superposition of octave, combined and differential absorption bands, which correspond to the fundamental frequencies of chemical bonds with high energies in an organic matter [12]. The NIRS can also reflect the composition information of the organic compounds containing hydrogen. It is very suitable for both qualitative and quantitative analyses of such hydrogen-containing organic compounds as agricultural, food and medical products.

In general, the NIRS can be used to determine the origin of such food as almonds [13], tea [14], apples [15], pine nuts [16], etc. It can also be devised for classifying animal fibres [17], bread drying [18], oranges [19], normal and mouldy chestnuts [20–22] and corn grain hardness [23]. The method can be successfully used to quantify the contents of protein [24], fatty acids [25], mould [24], sugar [22] and oil [25]. Moreover, it has been employed for evaluating seed vigour and damage, e.g., for wheat [26, 27], corns [28, 29] and hazelnuts [30, 31].

The aim of this study is to evaluate the shape and deficiencies of hazelnuts and examine the feasibility of NIRS-based determination of the protein content in shelled hazelnuts. First we collect the spectral information associated with hazelnuts using the NIRS and then construct their spectral database. The protein content is also directly measured using a chemometric method. A model for nondestructive detection and identification of the protein content in hazelnuts is elaborated. The influence of common data-preprocessing and spectral-band screening methods on the accuracy of our model is discussed. This improves its prediction accuracy.

Our study reveals that the convolutional neural-network systems MobileNetV2 and ResNet-50 can identify efficiently the defects of hazelnuts. The performance of ResNet-50 is higher than that of MobileNetV2. The accuracy and recall have been improved, so that the F1 score for Resnet-50 is larger than 97%. As a result, we have demonstrated that the NIRS technique can reliably detect the protein content in hazelnuts. A well-known partial least-squares (PLS) method has been used to work out our model, while the technologies of first derivative, second derivative and standard normal variate (SNV) preprocessing have been compared and analyzed. Uninformative-variable elimination (UVE), Monte Carlo uninformative-variable elimination (MCUVE) and random-frog band-selection methods have been used for this aim. Our experimental results have demonstrated that the final model grounded upon the first-derivative preprocessing and the MCUVE band selection has the best performance.

2. Materials and methods

Hazelnut samples "*Corylus heterophylla*" were collected from Yichun Area of Heilongjiang Province and "*C. heterophylla* × *C. avellana*" from Tieling area of Liaoning Province in 2020. The samples were stored in our laboratory at the temperatures below 15ºC and the relative air humidity less than 60%. Ventilation was ensured and exposure to light was avoided to prevent hazelnuts from mildew and hazel smell. Then, the hazelnuts were shelled.

A high-resolution Canon EOS 600D SLR camera was used in our experiments. In order to prevent the influence of external environment, a standard HQ-T60 light-source box was used. A D65 light source of this source box was consistent with the sunset light, which could imitate a natural light source under normal conditions. Under these conditions, we were able to reduce completely the impact of lighting and shooting factors on the experimental data.

In particular, to eliminate the influence of shooting angle on the experimental results, one had to meet the following conditions in the process of hazelnut-image collecting: when collecting a sample image, the equipment and the experimental sample were required to be at fixed positions, at a fixed distance and under a unified angle. Moreover, it was required that the focus was in the centre of the sample to ensure accurate focusing. In this way we tried to avoid the difficulties with image post-processing due to inaccurate focusing or blurred images. In our study, we adopted self-shooting. The shooting location was a laboratory at the Northeast Forestry University in Harbin, Heilongjiang Province. A total of 1085 images were taken.

The NIRS was used to evaluate our hazelnut samples. Before scanning them, the samples were stored at the laboratory for about 24 h to make their temperature and humidity consistent with those of the laboratory. After scanning, they were stored at –20ºC until the protein content was determined.

A NIR Quest512 spectrometer (American Ocean Company) was used for the NIRS experiments. It was equipped with a 512-element InGaAs array. The wavelength range was 900–1700 nm, the spectral resolution 3 nm, the response peak 1.6 μm, the signal-to-noise ratio 4000:1 (for full signal), and the integration time ranged from 1 ms to 10 s. Our equipment was able to measure

the reflectance (R) spectra, from which the absorbance A was obtained as $A = \log_{10}(1/R)$, supposing that the transmittance was small enough to be neglected. A calibrated 50% standard was used as a white reference before the measurements to prevent our detector from saturating during acquisition. The dark reference spectrum was obtained by covering the measuring head with all black.

During the measurements of the near-infrared spectra for hazelnuts, each sample was installed on a ring with a 6 mm-diameter opening, whereas a ring with a diameter 6 mm was fixed at the top (see Fig. 1). A diffuse reflection probe was placed parallel to the surface of hazelnuts as far as possible. Ten spectral values were obtained in each case and the average value was calculated. The spectral data were stored in MS Excel.

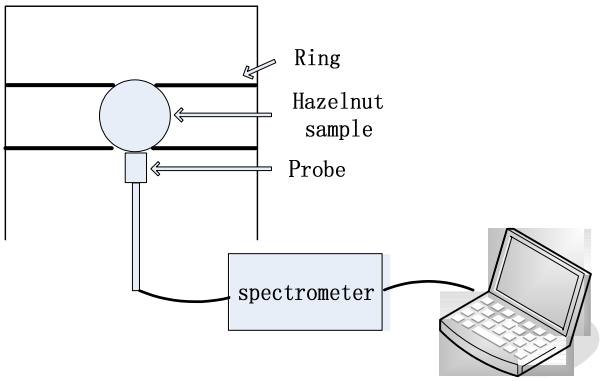

Fig. 1. NIRS acquisition system (see the texts for explanations).

The protein content in hazelnuts was determined with a Kjeldahl method (according to the first technique described in GB 5009.5-2016). During the spectroscopic experiments, each sample was measured three times, and the average was taken as an accurate value associated with the protein content in a given sample (see Table 1).

A Kennard–Stone method was used to select and make the calibration (training) set more representative, with a more uniform distribution and more reasonable division of the sample set. According to this method, the relative Euclidean distance in the sample spectral-data space was used to determine a subspectral space that represented a predetermined number of correction samples in the original data space to the greatest extent. First, the samples were uniformly selected in the feature space to conduct a principal-component analysis on the original spectral data. Then the principal-component score was selected as a characteristic variable to select the samples. The sample set was divided into a calibration (training) set and a verification (test) set according to the principle of 4:1. The results of this division are shown in Table 1.

Table 1. Protein partition results obtained for hazelnut samples.

Sample set	Number	Protein content, %		
		Maximum	Minimum	Average
Total sample set	185	24.01	11.07	18.14
Training set	148	24.01	11.07	18.21
Test set	37	20.87	12.23	17.77

3. Identification of hazelnut-kernel defects

3.1. Dataset preprocessing

According to the T/CSF 004-2019 hazelnut-quality grade, the hazelnut images collected in our experiments can be divided into three grades: full, incomplete and deformed (malformed). The relevant original images are shown in Fig. 2.

Fig. 2. Hazelnut images: full (a), incomplete (b) and malformed (c) hazelnuts.

The sizes of the images collected in our experiments are 5184×3456. Too large numbers of pixels would have affected the network-training speed, whereas a useful feature information is usually situated in the middle of the image. In order to reduce the amount of data calculations and the network-training time, we have chosen cropping the images, while ensuring retention of their key information. After noise reduction and clipping of images, they have been transformed to the gray scale.

3.2. Dataset enlarging and partitioning

A set of images taken in our experiments has been limited. To avoid fitting during the experiments, we have chosen to enlarge the dataset to a certain extent. This mainly implies random rotations and movements and mirror inversion of the initial images, as well as adding noise. In this manner we arrive at the situation when a limited image dataset is in fact equivalent to a larger final dataset without significant increase in the factual data amount.

The expanded dataset is divided according to the proportion 70:30. 4232 images are randomly selected as a training set, 2962 as a verification set, and 1270 as the validation set. This dataset division is illustrated in Table 2.

The training set is mainly used to train the parameters of our model. The validation set is responsible for testing the accuracy and loss rate of the model after each epoch is completed. After the validation performed on the validation set is completed, the model provides the training and validation data and starts the next round of epoch training. These procedures are repeated in a cycle until the end of 30 epochs.

Table 2. Dataset division.

Type of hazelnuts	Training set, pieces	Validation set, pieces	Dataset, pieces
Full	1184	495	1679
Incomplete	1007	387	1394
Malformed	771	388	1159

3.3. MoblieNetV2 network structure and analysis

MobileNetV2 is a new type of lightweight networks, which ensures high accuracy and reduces greatly computing and storage resources. A core part of the MobileNetV2 architecture is that it uses an inverted residual approach. The inverted residual block is different from the ordinary residual block in its structure. The difference is that when the input enters the residual structure,

the module increases the dimension of the data, increases the number of channels of the characteristic matrix, then carries out a depth-wise convolution on the increased-dimension data and finally reduces the dimension of the data. When compared with the ordinary residual structure, the inverted residual one chooses to increase the dimension first and then reduce it. Moreover, the two networks have certain differences in the selection of activation functions. The activation function for the fast use of the ordinary residuals represents a rectified linear unit (ReLU) function, while the function used for the cross-use of the inverted residuals is ReLU6 [17].

Using the MobileNetV2 network in training and recognizing 4232 images from our hazelnut-kernel defect dataset, we have obtained the following results: after 30 times of epoch training, the highest accuracy of the model-training set is 89.6% and the lowest loss rate equals to 0.044. The accuracy of the validation set amounts to 85.2% and the loss rate is 0.179. The training results of the MobileNetV2-model recognition are shown in Table 3. Fig. 3 displays the curves related to the model-training effect. It is seen from Fig. 3 that the model data converges quickly beginning from about epoch 9. The model-fitting effect is good and the model accuracy can be evaluated as fair. After the model training, we have calculated the precision and recall of the MobileNetV2 model for the three types of hazelnut samples (full, incomplete and malformed), as shown in Table 4.

As seen from Table 4, we have the highest accuracy rate for the malformed hazelnut kernels, the highest recall rate and the lowest accuracy occur for the full kernels. The recall rate for the hazelnuts of the incomplete type is the lowest, which proves that the model reveals the best recognition effect for the hazelnuts of abnormal types. At the same time, the recognition is somewhat poorer for the hazelnuts of the full and incomplete types. On the whole, we state that the recognition and classification abilities of our model are insufficient and cannot meet the requirements of processing and production.

Table 3. Training results obtained for the MobileNetV2-model recognition.

Method	Training accuracy	Training loss	Validation accuracy	Validation loss
MobileNetV2	89.68%	0.0422	85.23%	0.1785

Table 4. Accuracy and recall obtained for the MobileNetV2 method.

Method	Precision			Recall		
MobileNetV2	Full	Incomplete	Malformed	Full	Incomplete	Malformed
	0.84	0.90	0.90	0.90	0.84	0.87

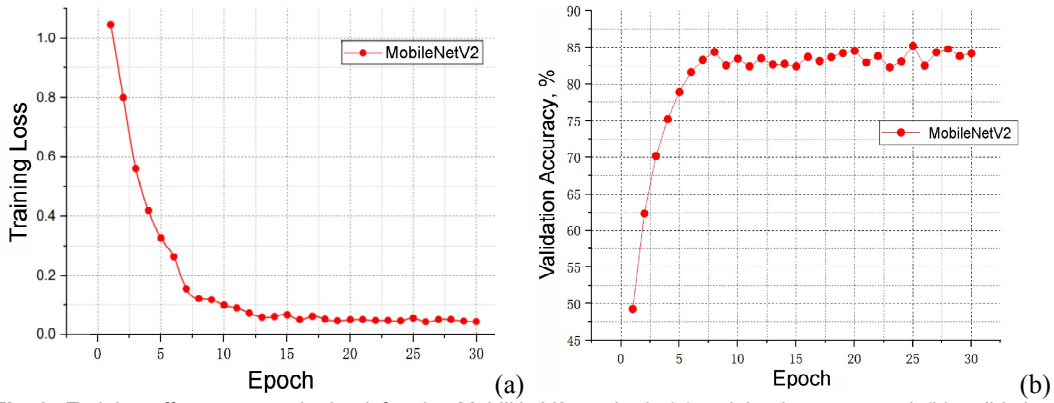

Fig. 3. Training-effect curves obtained for the MobilNetV2 method: (a) training-loss rate and (b) validation accuracy.

3.4. Resnet-50 network structure and analysis

Trying to solve the problem that the gradient disappears in deep learning and a deep network is difficult to train, we have adopted a Resnet-50 network model. Using Resnet-50 to train and recognize 4323 images from the hazelnut-kernel defect dataset, we have obtained the results shown in Table 5.

Table 5. Accuracy and recall obtained for the Resnet-50 method.

Method	Training accuracy	Training loss	Validation accuracy	Validation loss
Resnet-50	99.97%	0.0029	99.16%	0.0273

Fig. 4 displays the curves that illustrate the model-training effect. As seen from Fig. 4, the model converges rapidly beginning from about epoch 9. The curves of the training and validation accuracies are close to each other, the training and validation loss rates are described by relatively smooth curves, and the fitting effect of the model is good enough. The overall effect looks better than that of the training MobileNetV2 model. After the model training, we have calculated the accuracy and recall of the Resnet-50 model for the three types of hazelnut samples (see Table 6).

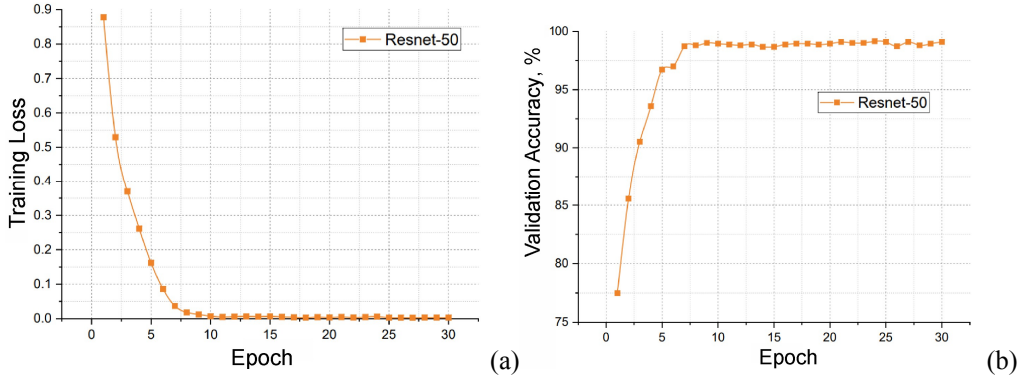

Fig. 4. Training-effect curves obtained for the Resnet-50 method: (a) training-loss rate and (b) validation accuracy.

Table 6. Accuracy and recall obtained for the Resnet-50 method.

Method	Precision			Recall		
Resnet-50	Full	Incomplete	Malformed	Full	Incomplete	Malformed
	0.99	0.96	0.99	0.99	0.99	0.97

3.5. Comparison of models

The main results of the MobileNetV2 and Resnet-50 models are gathered in Table 7 and Fig. 5. As compared with MobileNetV2, the training accuracy of Resnet-50 is improved by about 10.3% and the training loss rate is reduced by ~ 0.04. The prediction accuracy for the validation set increases by ~ 13.9% and the validation loss rate is reduced by ~ 0.15. In other words, the overall training effect is improved. At the same time, the absolute values of the accuracy, recall and F1 score for Resnet-50 are also significantly improved and reach more than 97%.

Table 7. Comparison of Resnet-50 and MobileNetV2 results.

Method	Training accuracy	Training loss	Validation accuracy	Validation loss
MobileNetV2	89.68%	0.0442	85.23%	0.1785
Resnet-50	99.97%	0.0029	99.16%	0.0273

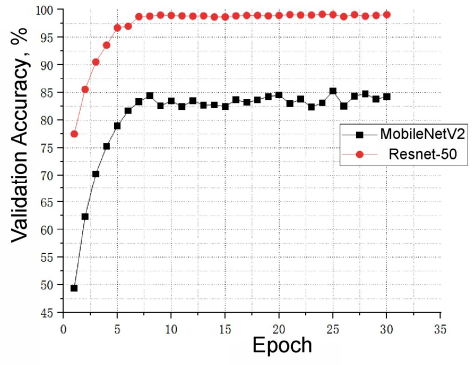

Fig. 5. Comparison of training processes for the Resnet-50 (full circles) and MobileNetV2 (full squares) methods.

4. NIRS data processing and analysis of results

4.1. Spectral analysis

The original spectral data obtained for hazelnuts are shown in Fig. 6 and Fig. 7. Here the wavelength range is 900–1700 nm and the sampling interval is equal to 1.57 nm. Protein is a substance with a complex spatial structure, of which main components are C, H, O and N. The main bands observed in the near-infrared range are those associated with the absorption of hydrogen-containing groups. The phenomenon of overlapping is also observed, i.e. multiple and combined fundamental frequencies can contribute to a given band. The original spectra of hazelnuts involve three principal peaks, as shown in Fig. 6 and Fig. 7. The first peak is located near 1180 nm, i.e. a combined frequency of the stretching vibration of the hydrogen-containing group [32]. The second peak is around 1420 nm, which corresponds to the first-order frequency doubling for the N–H group [33]. Finally, the third peak is located near 1660 nm, which represents a wavelet [34]. It refers to the first-order frequency doubling for the C–H and O–H groups. Although the absorption intensity in the near-infrared range is weak and different bands overlaps with each other, the shapes of the bands are highly regular and can reflect the information about the hazelnut protein.

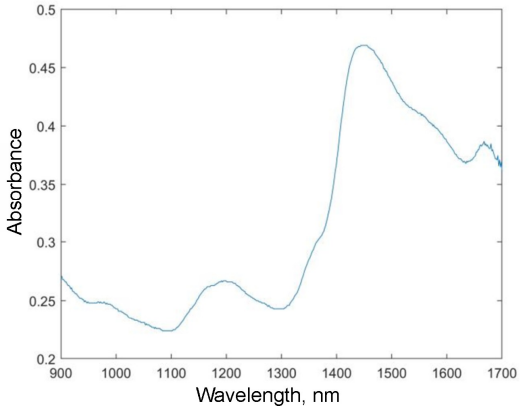

Fig. 6. Original absorbance spectra obtained for a single hazelnut sample.

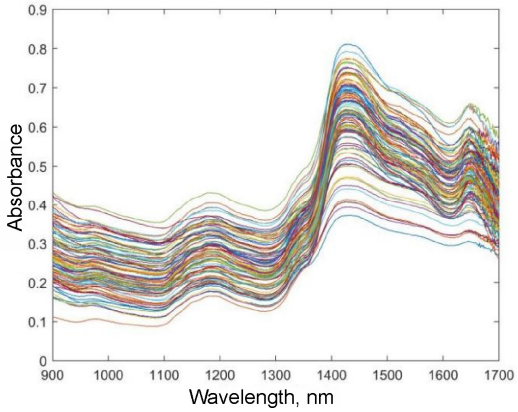

Fig. 7. Original absorbance spectra obtained for a group of hazelnut samples.

4.2. Spectral data preprocessing

Besides of the information on the basic chemical composition of samples, the spectral data collected by us contains also the information on individual samples, together with a considerable amount of background information and a noise. Therefore some preprocessing of the spectra is

necessary to reduce the spectral noise and eliminate the scattered light and influence of the optical-path change on the spectra. In this study, the first-derivative, second-derivative and SNV approaches are used to preprocess the spectra. The first two approaches imply a baseline correction, which can eliminate efficiently the background interference and the baseline drift or rotation, although they amplify the noise.

Fig. 8 shows the preprocessing results obtained with the first- and second-derivative methods. Here the ordinates are the first and second derivatives of the absorbance A. It is evident that the interference of baseline and the background in these spectra are eliminated.

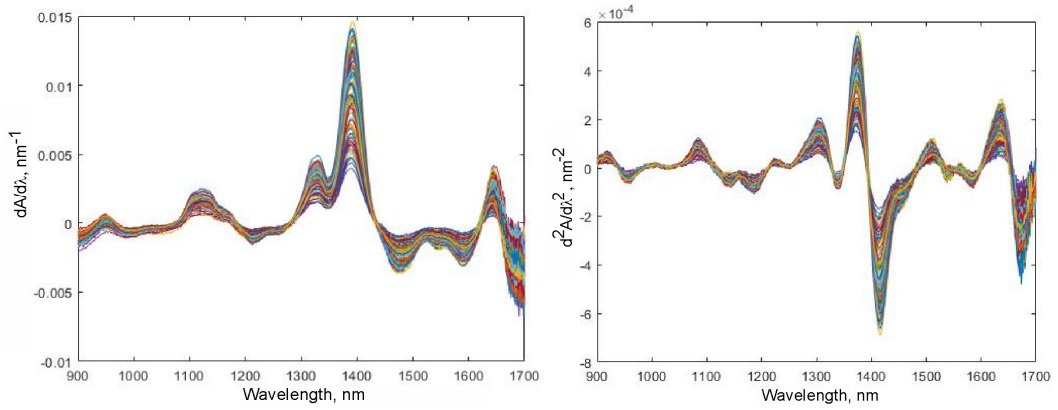

(a) (b)

Fig. 8. Results of preprocessing of the original absorbance spectra by the first-derivative (a) and second-derivative (b) methods.

The SNV is a method for correction of scattering. It subtracts the average value of the spectral absorbance from the original spectral signal and then divides it by the standard deviation of the spectrum obtained for the correction set. This can reduce the spectral difference caused by surface-dispersion characteristics and optical-path changes. Note that the calculation principle of the SNV involves the rows of the spectral array. Therefore, its processing effect is related to the spectral characteristics of individual samples. Fig. 9 shows the results of preprocessing performed using the SNV technique. After the SNV treatment, the coincidence of spectra obtained for different samples becomes higher and the influence of scattering is weakened.

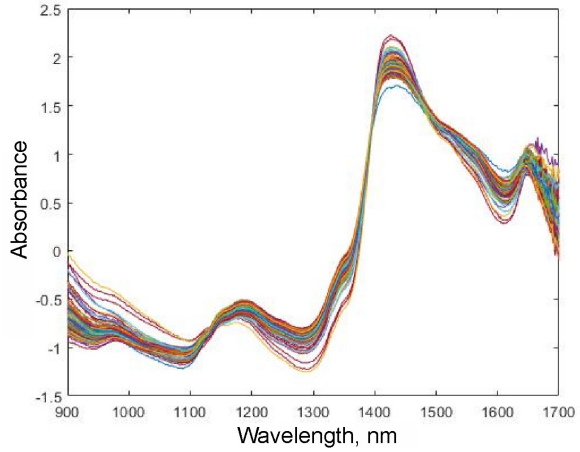

Fig. 9. Results of SNV preprocessing of the original absorbance spectra.

4.3. Selection of characteristic bands

The amount of full-band spectral data is too large to deal with. This data is associated with a lot of redundant information, so that heavy modelling and calculation workloads and long processing times would have been needed. Moreover, some frequency bands contain much noise, which makes the predictions unstable. Therefore, specific frequency bands (or spectral regions) should be selected for the modelling process.

The basic idea of the UVE technique for screening characteristic variables is to take the ratio of the average regression coefficient corresponding to a variable to its standard deviation as a measurement basis for selecting this variable. The related expression is given by

$$CV = \frac{\text{mean}(b_i)}{\text{Std}(b_i)}, \tag{1}$$

where b_i is the column vector of the spectral matrix. The final judgment method is to add a certain number of random-variable matrices to the spectral matrix, use the PLS method through cross-validation to obtain the regression-coefficient matrix and take the maximal CV value, $CV_{\max}$, of the random-variable matrix as a threshold. When the CV value corresponding to a variable is lower than $CV_{\max}$, the variable must be eliminated.

Fig. 10 shows the results of the UVE preprocessing for the band selection. We have ranked the importance of the near-infrared spectral bands according to the UVE algorithm and selected the first 20 bands. The red vertical lines in Fig. 10 indicate the characteristic bands filtered by us. It is readily seen from Fig. 10 that the selected wavelengths are relatively dense and there are no real absorption bands in the selected spectral regions. Therefore, this band-selection method cannot provide good results.

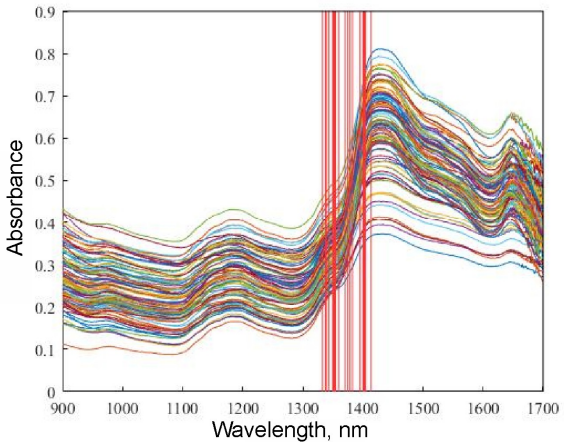

Fig. 10. UVE-based band selection in the original absorbance spectra.

The MCUVE method represents an improved version of the UVE. It adds a Monte Carlo sampling principle to the basic method for deleting uninformative variables. First, a variable-selection standard is set. The purpose of this standard is to calculate the stability of each variable and then determine whether we introduce this variable into the model or not, issuing from the relevant stability value. Then the root-mean-square error of prediction (RMSE-P) is calculated for selecting the variables to be retained. A number of variables corresponding to the smallest RMSE-P values are retained, thus establishing a PLS model. Fig. 11 shows the preprocessing results obtained by the MCUVE band-selection technique. The red vertical lines in Fig. 11 correspond to the characteristic wavelengths filtered with the MCUVE. The lines selected by the MCUVE method are concentrated in the region 1410–1580 nm, being located mainly around 1550 nm.

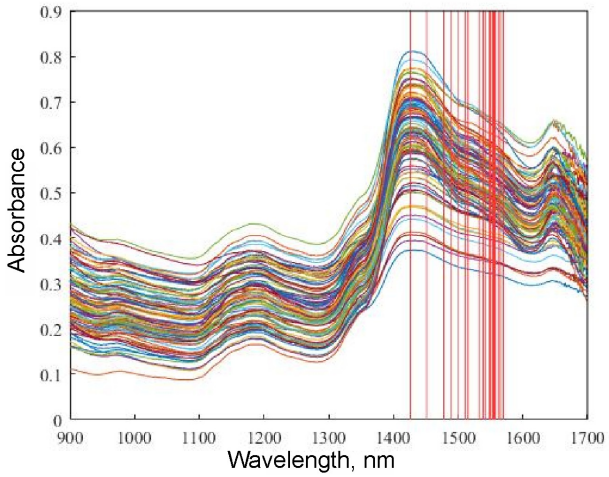

Fig. 11. MCUVE-based band selection in the original absorbance spectra.

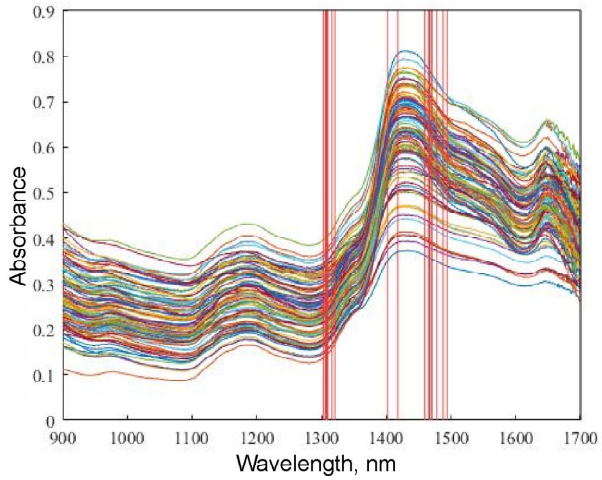

Fig. 12. Random-frog-based band selection in the original absorbance spectra.

The random-frog technique is a new characteristic-band algorithm. It uses a small number of variable iterations for modelling and represents an efficient tool for selecting the variables. Fig. 12 shows the preprocessing results obtained with the random-frog band-selection method. The vertical red lines in Fig. 12 represent the filtered characteristic wavelengths. The characteristic lines selected by the random-frog method are unevenly distributed near 1300 nm and between 1400 and 1500 nm.

4.4. Ascertaining a PLS method for NIRS

The calibration of the model has been carried out using the PLS method. The calibration has been validated with the method of full cross-validation. The minimal root-mean-square error of the cross-validation has been taken to avoid overfitting. We have used the root-mean-square error *RMSE* and the correlation coefficient *R* as evaluation parameters:

$$RMSE = \sqrt{\frac{\sum_{i=1}^{n}(y_i - y_m)^2}{n}}, \tag{2}$$

$$R=\frac{\sum_{i=1}^{n}(y_i-y_m)(y_i^{'}-y_m^{'})}{\sqrt{\sum_{i=1}^{n}(y_i-y_m)^2\sum_{i=1}^{n}(y_i^{'}-y_m^{'})^2}}, \quad (3)$$

where $y_i^{'}$ and $y_i^{'}$ are the individual sample points indexed by i and observed n times, and y_m and $y_m^{'}$ are the mean values.

4.5. Model validation

In this study, we have used the first-derivative, second-derivative and SVN methods to preprocess the original spectra. Table 8 shows the modelling results obtained after spectral preprocessing performed with different techniques. The correlation coefficient R_{test} for the test set is the largest with the first-derivative method. It reaches the value ~ 0.965. The RMSE-P for the first-derivative method is the smallest, ~ 0.577. The original spectra are characterized by the worst R_{test} value equal to ~ 0.579 and the smallest correlation coefficient which reaches only ~ 0.622. The original spectra also manifest the highest root-mean-standard error RMSE-C for the training set (~ 1.124). Finally, the highest root-mean-standard error for the test set found in the case of no spectral preprocessing (i.e., the original spectra) reaches the value ~ 1.365.

Table 8. Results of the PLS method obtained by different pretreatment techniques.

Pretreatment technique	Training set		Test set	
	$R_{training}$	RMSE-C	R_{test}	RMSE-P
Original spectra	0.6224	1.1238	0.5789	1.3652
First-order derivative	0.9377	0.2864	0.9654	0.5766
Second-order derivative	0.8632	1.0035	0.7322	1.0233
SNV	0.6592	0.9664	0.5403	1.0969

We have constructed the quantitative models using (i) the spectra of hazelnuts detected in the overall spectral range under test and (ii) the characteristic spectral bands selected by the UVE, MCUVE and random-frog methods. The optimal method for selecting the characteristic bands has been found by comparing the R and RMSE-P parameters. The evaluation results for different models are shown in Table 9. It is obvious from Table 9 that the methods of band screening improve the correlation coefficient and decrease the root-mean-square error. The results for the MCUVE-based method are the best, mainly because the characteristic bands screened by this technique correspond to the fundamental, doubled and combination frequencies of the protein bonds.

The main components of vegetable proteins are α-amino acids, which contain α-carbon atom, one H atom, one amino group and one side-chain R group. There are 20 different α-polypeptide polymers composed of amino acids and amino acids linked by different peptide bonds, e.g. C–H and N–H [35, 36]. The characteristic bands selected by the MCUVE method are mainly concentrated in the region 1427–1571 nm. In particular, there are 4 bands below 1500 nm (1427, 1452, 1479 and 1490 nm), which can be assigned to the combined C–H frequency [37]. The rest of the bands are between 1500 and 1571 nm, including those located at 1501, 1512, 1517, 1534, 1540, 1543, 1549, 1550, 1554, 1556, 1557, 1559, 1564, 1567 and 1571 nm. The first-order doubled-frequency absorption band corresponding to the stretching vibration of N–H bond is located near 1510 nm [38], which fits in the above characteristic bands. Hence, the most important absorption bands attributed to the proteins are retained, while most of the redundant variables are

eliminated. In case of the MCUVE band-selection, the correlation coefficient for the test set reaches 0.875 and the RMSE-P is 0.975.

Table 9. Model-valuation results obtained for different band-selection methods.

Band-selection method	Training set		Test set	
	$R_{training}$	RMSE-P	R_{test}	RMSE-P
Overall spectral range	0.7367	1.0447	0.7211	1.0226
UVE	0.8407	1.0223	0.8081	1.0880
MCUVE	0.9022	0.9667	0.8750	0.9753
Random frog	0.8843	0.9954	0.8597	0.9844

The data shown in Fig. 13 correspond to the model obtained by using simultaneously the first-derivative preprocessing method and the MCUVE band-selection method. A total of 10 hazelnuts not participating in the training have been randomly selected to predict the protein content in hazelnuts and evaluate the efficiency of our method and its actual prediction effect. The reference protein contents have been measured by the reliable chemical method. The difference between the measured and predicted protein contents has been calculated (see Table 10). The absolute errors of the protein contents for all the hazelnuts are less than 0.46 and the relative errors range from 0.19 to 2.37%, such that this error remains less than 2% for most of the samples. This demonstrates that our model provides an essentially accurate prediction and makes it feasible to detect the protein content in the hazelnuts using the NIRS. Fig. 13 testifies that the predicted protein-content values in the test set fluctuate around the chemically measured value and the fluctuation region is relatively small and uniform.

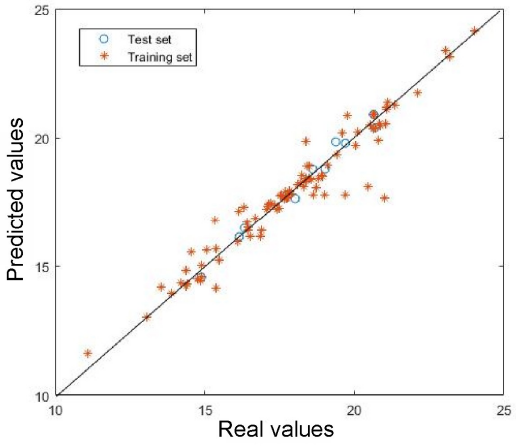

Fig. 13. Validation of PLS method.

Table 10. Hazelnut-protein contents chemically measured for 10 samples versus the corresponding values predicted by our MCUVE–PLS model.

Sample number	Value measured by the chemical method, %	Value predicted from our spectral method, %	Absolute error	Relative error, %
1	20.70	20.39	0.31	1.50
2	16.33	16.47	0.14	0.86
3	18.02	17.64	0.38	2.11
4	14.88	14.56	0.32	2.15
5	19.70	19.79	0.09	0.46
6	19.38	19.84	0.46	2.37
7	16.15	16.12	0.03	0.19
8	20.64	20.90	0.26	1.26
9	18.61	18.78	0.17	0.91
10	19.02	18.79	0.23	1.21

5. Conclusions

Let us summarize the main results of the present study.

1. The MobileNetV2 and Resnet-50 neural-network models have been used for identification of the defects in hazelnut kernels. Basing on comparison of the training results obtained with the two networks, we have found that the prediction accuracy for the Resnet-50 training set is 10.3% higher than that of MobileNetV2 and the training loss rate is reduced by 0.041. Under the same conditions, the validation accuracy is improved by 13.9% and the validation loss rate is lowered by 0.151. In other words, the overall training effect of the Resnet-50 neural network is notably better than that of MobileNetV2.

2. The correlation coefficient R_{test} for the test set becomes the largest (0.965 at the most) if one employs the first-derivative preprocessing technique. Then the parameters RMSE-P and RMSE-C are the smallest (0.577 and 0.2864 for the test and training sets, respectively).

3. The correlation coefficients for the hazelnut spectra preprocessed using the second-derivative for the training and test sets are respectively equal to 0.863 and 0.732. The same figures obtained with the SNV technique are 0.659 and 0.543 for the training and test sets, respectively. The results following from the SNV-preprocessed spectra are similar to those of the original spectra, thus indicating that this preprocessing method had a limited ability to extract efficiently the spectral information.

Note that Hongbo Li et al. in their recent work [39] have studied the problems similar to those of our work. Namely, they have analyzed the methods for determining the concentration of lipids in pine nuts, using the NIRS in the range of 900–1700 nm. Since the nutrient components of the hazelnuts and pine nuts are relatively close, the spectra [39] are similar to our data.

Acknowledgements

This work was supported in part by the Fundamental Research Funds for the Central Universities (the Grant #2572019BF02) and the Program of National Natural Science Foundation of China (CN) (the Grant #31700643).

References

1. Neus B, Cháfer M, Chiralt A and González-Martínez C, 2014. Hazelnut milk fermentation using probiotic Lactobacillus rhamnosus GG and inulin. Int. J. Food Sci. Technol. **49**: 2553–2562.
2. Giovanna Canneddu, Luis Carlos Cunha Junior and Gustavo Henrique de Almeida Teixeira. 2016. Quality evaluation of shelled and unshelled macadamia nuts by means of near-infrared spectroscopy (NIR). J. Food Sci. **81**: 1613–1621.
3. Pannico A, Schouten R E, Basile B, Romano R, Woltering E J and Cirillo C, 2015. Non-destructive detection of flawed hazelnut kernels and lipid oxidation assessment using NIR spectroscopy. J. Food Engin. **160**: 42–48.
4. Venkatachalam M and Sathe S K, 2006. Chemical composition of selected edible nut seeds. J. Agricult. Food Chem. **54**: 4705–4714.
5. Delgado T, Malheiro R, Alberto Pereira J and Ramalhosa E, 2010. Hazelnut (Corylus avellana L.) kernels as a source of antioxidants and their potential in relation to other nuts. Indust. Crops Prod. **32**: 621–626.
6. Ayvaz H, Temizkan R, Efe Genis H, Mortas M, Genis D O, Dogan M A, Nazlim B A, 2022. Rapid discrimination of Turkish commercial hazelnut (Corylus Avellana L.) varieties using near-infrared spectroscopy and chemometrics. Vibr. Spectrosc. **119**: 103353.

7. He Yizhi, Zhu Tiancheng, Wang Mingxuan and Lu Hanqing, 2021. On lemon defect identification with visual feature extraction and transfers learning. J. Data Analysis Inform. Process. **9**: 233–248.
8. Li Cong, Yu Guowei, Zhang Yuanjia and Ma Benxue, 2022. Research on recognition of stem/calyx and defects of dried Hami jujube based on ResNeXt and transfer learning. Food & Machinery. **38**: 135–140.
9. Liying Fan, Jun Ren, Yuting Yang and Limin Zhang, 2020. Comparative analysis on essential nutrient compositions of 23 wild hazelnuts (Corylus heterophylla) grown in Northeast China. J. Food Qual. **2020**: 9475961.
10. Levinson L R and Gilbride K A, 2011. Detection of melamine and cyanuric acid in vegetable protein products used in food production. J. Food Sci. **76**: C568–C575.
11. Ji Xiao-fei, You Ming-hong, Bai Shi-qie, Li Da-xu, Lei Xiong, Wu Qi, Chen Li-min, Zhang Chang-bing, Yan Jia-jun, Yan Li-jun, Chen Li-li and Zhang Yu, 2019. Establishment of quantitative model for analyzing crude protein in phalaris arundinacea L. by near infrared spectroscopy (NIRS). Spectrosc. Spectr. Analysis. **39**: 1731–1735.
12. Chu X L, Xu Y-P and Lu W-Z, 2008. Research and application progress of chemometrics methods in near infrared spectroscopic analysis. Chin. J. Analyt. Chem. **36**: 702–709.
13. Arndt M, Rurik M, Drees A, Bigdowski K, Kohlbache O and Fischer M, 2020. Comparison of different sample preparation techniques for NIR screening and their influence on the geographical origin determination of almonds (Prunus dulcis MILL). Food Control. **115**: 107302.
14. Ming-Zhi Zhu, Beibei Wen, Hao Wu, Juan Li, Haiyan Lin, Qin Li, Yinhua Li, Jianan Huang and Zhonghua Liu, 2019. The quality control of tea by near-infrared reflectance (NIR) spectroscopy and chemometrics. J. Spectrosc. **2019**: 8129648.
15. Eisenstecken D, Stürz B, Robatscher P, Lozano L, Zanella A and Oberhuber M, 2019. The potential of near infrared spectroscopy (NIRS) to trace apple origin: Study on different cultivars and orchard elevations. Postharvest Biol. Technol. **147**: 123–131.
16. Veronica Loewe M, Navarro R M, Cerrillo R M, Cerrillo N, Garcia-Olmo J, Garcia-Olmo J and Sánchez-Cuesta R, 2017. Discriminant analysis of Mediterranean pine nuts (Pinus pinea L.) from Chilean plantations by near infrared spectroscopy (NIRS). Food Control. **73**: 634–643.
17. Chen H, Lin Z and Tan C, 2019. Classification of different animal fibers by near infrared spectroscopy and chemometric models. Microchem. J. **144**: 489–494.
18. Swathi Sirisha Nallan Chakravartula, Chiara Cevoli, Balestra F, Fabbri A, Dalla Rosa M, 2019. Evaluation of drying of edible coating on bread using NIR spectroscopy. J. Food Engin. **240**: 29–37.
19. Pérez-Marín D, Calero L, Fearn T, Torres I, Garrido-Varo A and Sánchez M-T, 2019. A system using in situ NIRS sensors for the detection of product failing to meet quality standards and the prediction of optimal postharvest shelf-life in the case of oranges kept in cold storage. Postharvest Biol. Technol. **147**: 48–53.
20. Moscetti R, Monarca D, Cecchini M, Ron P Haff, Contini M and Massantini R, 2014. Detection of mold-damaged chestnuts by near-infrared spectroscopy. Postharvest Biol. Technol. **93**: 83–90.
21. Moscetti R, Ron P Haff, Sirinnapa Saranwong, Monarca D, Cecchini M and Massantini R, 2014. Nondestructive detection of insect infested chestnuts based on NIR spectroscopy. Postharvest Biol. Technol. **87**: 88–94.

22. Jiaqi Hu, Xiaochen Ma, LinglingLiu, Yanwen Wu and Jie Ouyang, 2017. Rapid evaluation of the quality of chestnuts using near-infrared reflectance spectroscopy. Food Chem. **231**: 141–147.
23. Williams P J and Kucheryavskiy S, 2016. Classification of maize kernels using NIR hyperspectral imaging. Food Chem. **209**: 131–138.
24. Schönbrodt T, Mohl S, Winter G and Reich G, 2006. NIR spectroscopy-a non-destructive analytical tool for protein quantification within lipid implants. J. Control Release. **114**: 261–267.
25. Cayuela-Sanchez J A and Palarea-Albaladejo J, 2019. Olive oil nutritional labeling by using Vis/NIR spectroscopy and compositional statistical methods. Innov. Food Sci. Emerg. Technol. **51**: 139–147.
26. Hacisalihoglu G, Freeman J, Armstrong P R, Seabourn B W, Porter L D, Settles A M and Gustin J L, 2020. Protein, weight, and oil prediction by single-seed near-infrared spectroscopy for selection of seed quality and yield traits in pea (Pisum sativum). J. Sci. Food Agricult. **100**: 3488–3497.
27. Fan Y, Ma S and Wu T, 2020. Individual wheat kernels vigor assessment based on NIR spectroscopy coupled with machine learning methodologies. Infrar. Phys. Technol. **105**: 103213.
28. Barbedo J G A, Guarienti E M and Tibola C S, 2018. Detection of sprout damage in wheat kernels using NIR hyperspectral imaging. Biosyst. Engin. **175**: 124–132.
29. Zhang J, Dai L and Cheng F, 2019. Classification of frozen corn seeds using hyperspectral VIS/NIR reflectance imaging. Molecules. **24**: 149.
30. Moscetti R, Haff R P, Aernouts B, Saeys W, Monarca D, Cecchini M and Massantini R, 2013. Feasibility of Vis/NIR spectroscopy for detection of flaws in hazelnut kernels. J. Food Engin. **118**: 1–7.
31. Tuncil Y E, 2020. Dietary fibre profiles of Turkish Tombul hazelnut (Corylus avellana L.) and hazelnut skin. Food Chem. **316**: 126338.
32. Navid Shakiba, Annika Gerdes, Nathali Holz, Soeren Wenck, René Bachmann, Tobias Schneider, Stephan Seifert, Markus Fischer, Thomas Hackl, 2022. Determination of the geographical origin of hazelnuts (Corylus avellana L.) by near-Infrared spectroscopy (NIR) and a low-level fusion with nuclear magnetic resonance (NMR). Microchem. J. **174**: 107066.
33. Jiaqi Hu, Xiaochen Ma, Lingling Liu, Yanwen Wu and Jie Ouyang, 2017. Rapid evaluation of the quality of chestnuts using near-infrared reflectance spectroscopy. Food Chem. **231**: 141–147.
34. Moscetti R, Haff R P, Saranwong S, Monarca D, Cecchini M and Massantini R, 2014. Nondestructive detection of insect infested chestnuts based on NIR spectroscopy. Postharvest Biol. Technol. **87**: 88–94.
35. Zhou R B. Functional Principle and Technology of Plant Protein. Beijing: Chemical Industry Press, 2007.
36. Yan Y L. Basis and Application of Near Infrared Spectroscopy. Beijing: China Light Industry Press, 2005.
37. Fan W, Shan Y, Li G, Lv H, Li H and Liang Y, 2012. Application of competitive adaptive reweighted sampling method to determine effective wavelengths for prediction of total acid of vinegar. Food Analyt. Meth. **5**: 585–590.
38. Zhao Lihua, Gong Yuanyong, Zhang Jie, Lin Zhangbin, Wang Ying, Li Xuewu, Dai Xun and Jiang Yun, 2020. Rapid determination of quinoa seeds crude protein content using near infrared spectroscopy. Sci. Technol. Food Industry. **41**: 233–236.

39. Hongbo Li, Dapeng Jiang, Jun Cao and Dongyan Zhang, 2020. Near-infrared spectroscopy coupled chemometric algorithms for rapid origin identification and lipid content detection of Pinus Koraiensis seeds. Sensors. **20**: 4905.

Dandan Li, Dongyan Zhang, Dapeng Jiang, Jun Cao and Jiuqing Liu. 2022. Hazelnut quality detection based on deep learning and near-infrared spectroscopy. Ukr.J.Phys.Opt. **23**: 267 – 283. doi: 10.3116/16091833/23/4/267/2022

Анотація. *Ядра фундука часто можуть бути неповними або деформованими та мати деякі інші дефекти. Ручні методи їхньої класифікації та розпізнавання або навіть застарілі підходи машинного навчання виявляють низьку ефективність розпізнавання та високий рівень неправильних оцінок. У цьому дослідженні ми застосували глибоке навчання до розпізнавання дефектів ядра фундука. Для навчання та розпізнавання використано дві згорткові нейромережеві системи MobileNetV2 і Resnet-50. Виявлено, що точність передбачення ResNet-50 для навчального набору покращена на 10,3%, а коефіцієнт втрат навчання зменшений на 0,041, порівняно з MobileNetV2. Крім того, точність перевірки, досягнута за допомогою ResNet-50, вища на 13,9%, а коефіцієнт втрат перевірки нижчий на 0,151. Це доводить, що загальний тренувальний ефект для нейронної мережі Resnet-50 кращий, ніж для MobileNetV2. За допомогою методу спектроскопії поглинання в близькому інфрачервоному діапазоні нами також вивчено вміст білка в фундуку, який є важливим параметром для оцінки його якості. Для класифікації вибірки використано алгоритм Кеннарда–Стоуна. Щоб розробити методику кількісного аналізу білка в фундуку, використано метод часткових найменших квадратів. Відповідні спектральні дані попередньо оброблено за методами першої похідної, другої похідної та стандартної нормальної змінної. Порівняно вплив цих методів на точність. Результати демонструють, що модель, заснована на першій похідній, є найкращою у разі даних, які стосуються всього спектрального діапазону. Коефіцієнти кореляції для навчальної та тестової вибірок дорівнюють відповідно 0,938 і 0,965, тоді як середньоквадратичні похибки для цих вибірок становлять відповідно 0,286 і 0,577. Наше дослідження засвідчує, що вміст білка в фундуку можна швидко виявити неруйнівним методом за допомогою близької інфрачервоної спектроскопії.*

Ключові слова: *нейронні мережі, глибоке навчання, метод часткових найменших квадратів, спектроскопія близького інфрачервоного діапазону, неруйнівний контроль, вміст білка*